BUCKLING BEHAVIOUR OF THE STEEL PLATE IN STEEL – CONCRETE – STEEL SANDWICH COMPOSITE TOWER FOR WIND TURBINE

Yu-Hang Wang [1], Shu-Qi Wang [2], Xu-Hong Zhou [1], Ji-Ke Tan [3, *], Jiu-Lin Bai [1] and Ke Ke [1]

[1] *School of Civil Engineering, Chongqing University, Chongqing, China*

[2] *Northwest Electric Power Design Institute Co., Ltd. of China Power Engineering Consulting Group, Xian, China*

[3] *Department of Civil Engineering, Tsinghua University, Beijing, China*

* (Corresponding author: E-mail: tjk23@sina.com)

A B S T R A C T

To solve the problem of collapses caused by local buckling of steel plates under compression in traditional steel towers, a novel steel-concrete-steel (SCS) sandwich composite tower for a wind turbine is proposed in this paper. To study the buckling behaviour of steel plates in SCS sandwich composite towers, six specimens were designed and tested under axial compression. The specimens were designed considering the key parameters of curvature radius, thickness of the steel plate, and the spacing-to-thickness ratio (the ratio of stud spacing to the thickness of steel plate). The failure modes, normalised average stress-strain curves and load-strain curves of the specimens were assessed, and the effects of the curvature radius and the spacing-to-thickness ratio of the steel plate were analysed. The experimental results showed that the buckling strength of the steel plate increased with a decrease in the ratio of the curvature radius to the thickness of the steel plate. The finite element (FE) model of the elastic buckling stress of the steel plate of the SCS sandwich composite tower was employed and validated against the test results. In parametric study, the effects of governing parameters including the curvature radius of the steel plate, thickness of the steel plate and spacing of the studs, on the effective length factors of the inner and outer steel plates were analysed. Subsequently, the design rules of the effective length factor of the inner and outer steel plates, and the design methods of spacing of studs to prevent local instability of the inner and outer steel plates before yielding were proposed.

1. Introduction

Wind energy is a type of clean renewable energy, and wind power generation is the most widely used and fastest-growing new energy generation technology. As the main load-bearing structure of the wind turbine, the tower not only supports the weight of the nacelle and rotor, but also bears the wind and dynamic loads. Therefore, the tower plays an important role in the stable operation of the entire wind turbine. Currently, steel towers are the most common form of wind turbine support structures because of their simple structure, high construction efficiency, and good safety. The steel tower is a large-size thin-walled steel tube structure that is very sensitive to initial imperfections. Under compression, the minor imperfections in the steel tower structure may cause local buckling or even collapse, as shown in Fig. 1 [1]. Once the tower collapses, it causes significant economic losses.

Fig. 1 Steel tower collapse accident caused by instability failure

It is well known that steel plates in concrete-filled steel tube (CFST) structures have better stability than traditional steel tubular structures [2-3]. Therefore, to solve the problem of collapse caused by local buckling of steel plates under compression in traditional steel towers, a novel steel-concrete-steel (SCS) sandwich composite tower for a wind turbine is proposed in this paper, as shown in Fig. 2. The inner and outer steel plates of the SCS sandwich composite tower are connected to the concrete through studs, which have a constraining effect on the concrete, and the concrete plays an out-of-plane support role on the steel plate, which can give full play to the material advantages of both concrete and steel. Therefore, the buckling capacity of the steel plate in the SCS sandwich composite tower is higher than that of the steel plate in the steel tower. In the design of the tower structure, as shown in Fig. 3, six types of loads should be considered: the gravity load of the wind wheel and engine room (G_1), eccentric bending moment (M_{YT}), aerodynamic thrust (F_{XH}),

and torque (M_{XH}) caused by the wind wheel and engine room, gravity load of the tower (G_2) and transverse wind load of the tower ($q(z)$). Under the combined action of the aforementioned six types of loads, the inner and outer steel plates at the bottom section of the composite tower with greater compressive stress may suffer local instability failure, which will affect the safety of the tower structure. Therefore, the compression stability of the steel plate at the bottom of the tower is of great significance for structural safety. In this study, to make full use of the mechanical properties of the steel plate material and ensure that the steel plate does not buckle before yielding, the local stability behaviour of the steel plate in the SCS sandwich composite tower under axial compression was investigated. This study aims to provide a theoretical basis for the application of SCS sandwich composite structures for wind turbine.
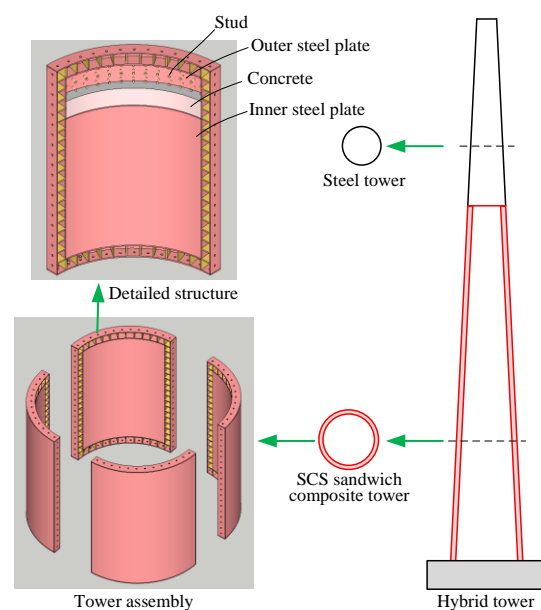

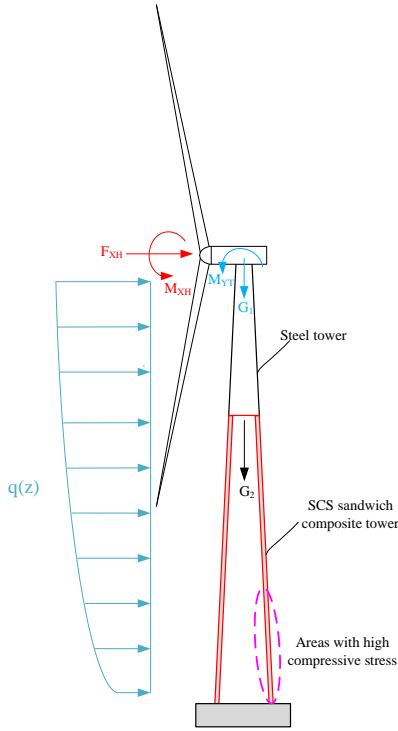**Fig. 2** Schematic diagram of SCS sandwich composite tower

Fig. 3 Load diagram of a new type of hybrid tower

There have been many studies on the buckling performance of steel plates of SCS sandwich composite structures [4-6]. Choi et al. [7-9] conducted an axial compression test of steel plate-concrete wall structures, and the experimental results showed that local buckling of the steel plate occurred between adjacent studs. When the spacing-to-thickness ratio was relatively large, increasing the yield strength of the steel plate has little effect on the compression strength of the steel plate. In addition, the buckling coefficient and the effective length factor of the steel plate were studied based on the plate theory and column theory, respectively, and a simplified formula for calculating the critical elastic buckling stress of the steel plate was proposed. Yan et al. [10] proposed a new type of SCS sandwich composite wall and completed eight axial compression tests. Based on the test results, a theoretical model of the wall compressive strength under different connection modes was established. The effective length factor was determined to be 0.825 by summarizing the 62 test results. Yang et al. [11] carried out 10 axial compression tests on double-skin composite wall specimens considering the influence of stud arrangement and spacing-to-thickness ratio. Based on the test results, they proposed a formula for limiting the spacing-to-thickness ratio to prevent local instability of the steel plates. Uy et al. [12-13] studied the buckling behaviour of steel plates of steel-concrete composite members by using the finite strip model, and proposed a design method for determining the buckling coefficient and effective length factor of steel plates, as well as a design method for selecting the width-thickness ratio of the steel plate. Cai et al. [14] theoretically investigated the elastic local buckling of steel plates in rectangular CFST columns with restraint bars under axial compressive loads. Furthermore, they derived the formula for calculating the critical stress of elastic buckling of steel plate is derived by using the energy method. They also determined the limit values for the spacing of restraint bars, the width-height ratio, and the width-thickness ratio to ensure that local bucking failure of steel plate does not occur before the steel plate yielding. Hu et al. [15]

conducted axial compression tests on 12 square CFST columns with restraint bars, and the loads were only applied on the steel plates. The influences of the width-to-thickness ratio of the steel plate and the ratio of the vertical spacing of the tie bars to the width of the steel plate on the stability performance of the steel plate were studied. Based on the FE parameter analysis results, a calculation method for steel plate buckling coefficient was proposed.

Previous studies on SCS sandwich composite structures mainly focused on the buckling behaviour of steel plates under axial loads, while there are few studies on the stability of steel plates when the axial load is only applied to the steel plate in the SCS sandwich composite structure. In addition, no relevant reports are available on the buckling behaviour of SCS composite sandwich tower structure under axial compression. Therefore, to study the stability performance of the steel plate under axial compression of the SCS sandwich composite tower structure proposed in this paper, six specimens were designed with curvature radius and spacing-to-thickness ratio as the key parameters. In the tests, the axial load was only applied to the steel plate, while the concrete only acted as the out-of-plane support for the steel plate without bearing any load. The buckling behaviour of the steel plate of the composite tower was investigated, and the design rules of the effective length factor and the design methods of spacing of studs to prevent local instability of the inner and outer steel plates before yielding were elucidated. The outcome of this study provides a theoretical basis and design guidance for the application of the SCS sandwich composite structure for wind turbines.

2. Experimental study

2.1. Specimens

Owing to the limitation of the size and loading capacity of the test device, only a partial structure of the composite tower was selected for the design of the test specimens. In this study, six specimens were designed with a height of 1000 mm and a core concrete thickness of 100 mm. The inner and outer steel plates of the SCS sandwich composite structure specimens were connected to the concrete through studs. The diameter and length of all the studs are 13 mm and 60 mm, respectively. A 12 mm thick endplate was welded at the upper and lower ends of the specimens, and the section centroid of the steel plate coincided with the endplate centroid. Detailed parameter information for the specimens is shown in Fig. 4 and Table 1. The grade of concrete of all specimens was C30, and the grade of the steel material was Q235. The average measured 28-day compressive strength of the concrete cube was 37.3 MPa. Tensile coupon tests of steel plates were carried out, and the measured steel plates material properties are listed in Table 2.
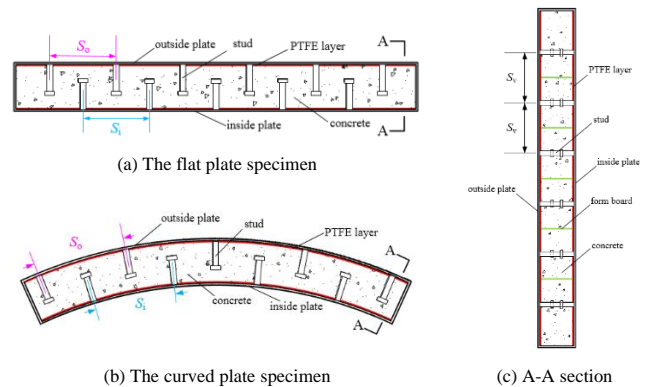

(a) The flat plate specimen

(b) The curved plate specimen

(c) A-A section

Fig. 4 Dimensions and detailed information of specimens

Table 1

Detailed parameters of specimens

Specimens	Concrete	Studs	R_i (mm)	R_o (mm)	t (mm)	S_i (mm)	S_o (mm)	S_v (mm)	S_v/t (-)	ρ (mm)
SPB1	-	-	1000	1100	2.45	-	-	-	-	7
SPB2	Yes	Yes	1000	1100	2.30	244	269	250	109	30
SPB3	Yes	Yes	1000	1100	4.70	147	161	150	32	10
SPB4	Yes	Yes	1000	1100	2.30	147	161	150	65	27
SPP1	Yes	Yes	∞	∞	2.28	150	150	150	66	25
SPP2	Yes	-	∞	∞	2.31	-	-	-	-	0

where, R_i is the curvature radius of the inner steel plate, R_o the curvature radius of the outer steel plate, t is the thickness of the steel plate, S_i is the spacing of studs on the inner steel plate along the arch direction, S_o is the spacing of studs on the outer steel plate along the arch direction, S_v is the spacing of studs on the inner and outer steel plates along the height direction, S_v/t is the spacing-to-thickness ratio of the steel plate, and ρ is the distance between the load point and centroid of the section.

Table 2
Mechanical properties of steel materials

Thickness (mm)	Yield strength (MPa)	Ultimate strength (MPa)	Modulus of elasticity (GPa)
2.5	332	455	189
5.0	298	458	199

As illustrated in Fig. 4, to prevent the axial load from acting on the concrete, a polytetrafluoroethylene layer with a very small elastic modulus was placed between the steel plate and the concrete, and a series of 10 mm thick form boards were placed between the adjacent studs to cut off the vertical force path of the concrete. To accurately control the height of each layer of concrete and facilitate placing of the boards, a series of 50 mm × 50 mm holes were reserved at the design height of the side plate of the specimen. After the concrete was poured, the hole was welded shut with a small steel plate. The specimen preparation process is illustrated in Fig. 5.
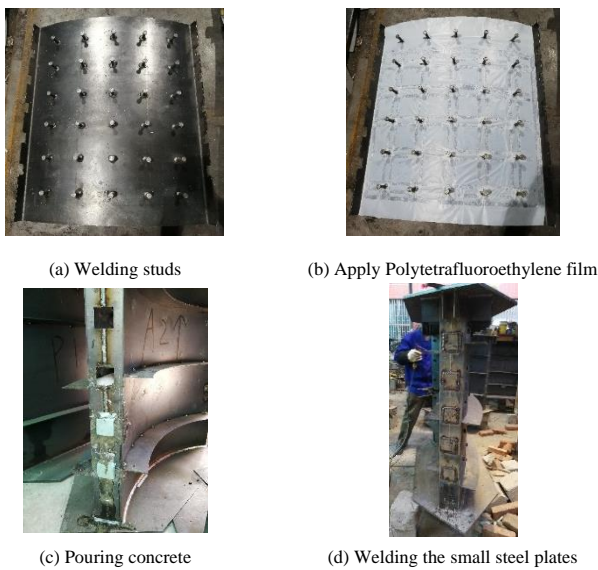

(a) Welding studs

(b) Apply Polytetrafluoroethylene film

(c) Pouring concrete

(d) Welding the small steel plates

Fig. 5 Fabrication process of specimens

2.2. Testing programme

(a) Loading device

(b) Arrangements of displacement meters

(c) Strain gauges arrangement of inner steel plate

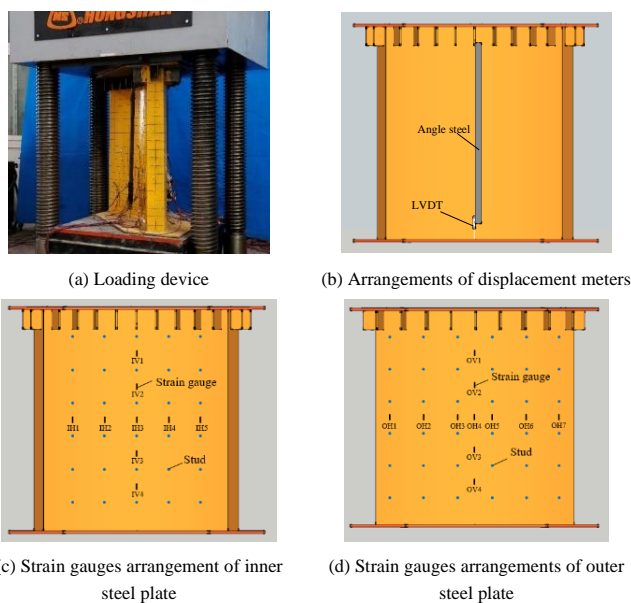(d) Strain gauges arrangements of outer steel plate

Fig. 6 Test setup and instrumentation plan

Compression tests were conducted using servo-controlled electrohydraulic testing machine. The test device and measurement scheme are shown in Fig. 6. The axial force applied to the specimens was measured by the force sensor of the device, and the axial deformation of the specimens was measured using

linear variable differential transformers (LVDTs) arranged symmetrically at the centre of the inner and outer steel plates (see Fig. 6b). To capture the strain change of the steel plate during the entire loading process and analyse the stress of the inner and outer steel plates, vertical strain gauges were arranged in the middle of the specimens along the horizontal and vertical directions, as shown in Figs. 6c and 6d. Before testing, the specimens were preloaded to 10% of the nominal bearing capacity (equal to $f_y A_s$) to check whether the specimens were uniformly stressed and whether the displacement measurement worked properly. The test was conducted using displacement control, and when the specimens were severely damaged or the load dropped to below its 85% of the peak strength of the specimens, the tests were terminated.

3. Experiments and analysis

3.1. Structural behaviours and failure modes

The failure modes of all specimens are shown in Fig. 7. As presented in Fig. 7a, in the early stage of loading, the specimen SPB1 was approximately in the elastic stage. During the loading process, when the load reached approximate $0.65N_m$ (N_m, the corresponding peak load of the specimens), the upper left part of the outer steel plate exhibited local buckling. When continuing to load to $0.72N_m$, local buckling appeared in the middle and lower parts of the inner steel plate. When the load continued to increase, the lower left part of the inner steel plate buckled. When the load reached the peak load N_m, the specimen made a loud noise and the load began to drop very quickly. When the load continued to increase, local buckling appeared near the mid-height of the outer steel plate, the lower right side of the inner steel plate and the left side of the inner and outer steel plates buckled.

For specimen SPB2, when the load reached approximately $0.92N_m$, the inner steel plate first began to buckle; then the steel plate buckled below the first row of studs on the upper left of the outer steel plate. When the load reached the peak load N_m (i.e. 771.4 kN), the curve at the upper left of the outer steel plate was pulled through, and three intervals of studs on the upper left of the inner steel plate buckled. When the load continued to increase, the upper right of inner steel plate began to buckle, and the steel plate on the top of the left plate and right plate buckled. The final failure mode of specimen SPB2 is shown in Fig. 7b.

As shown in Figs. 7c and 7d, the specimens SPB3 and SPB4 had similar failure modes, and the buckling positions of the inner and outer steel plates of specimens SPB3 and SPB4 were almost at the same height as the specimen. When loaded to $0.9N_m$, the first row of studs on the upper right of the outer steel plate buckled, and the first row of the studs of the inner steel plate also began to buckle. When the load reached N_m, the curve at the upper right of outer steel plate was pulled through, and the curve in the second row of the inner steel plate was pulled through between the horizontal studs. When the load continued to increase, the curve on the inner and outer steel plates was pulled through the left and right side plates.
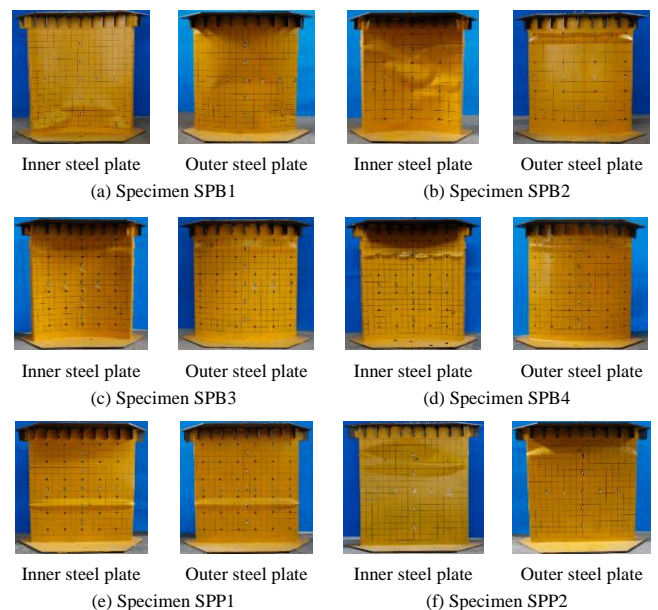

Inner steel plate | Outer steel plate | Inner steel plate | Outer steel plate
(a) Specimen SPB1 | (b) Specimen SPB2

Inner steel plate | Outer steel plate | Inner steel plate | Outer steel plate
(c) Specimen SPB3 | (d) Specimen SPB4

Inner steel plate | Outer steel plate | Inner steel plate | Outer steel plate
(e) Specimen SPP1 | (f) Specimen SPP2

Fig. 7 Failure modes of the specimens obtained from test

Specimens SPP1 and SPP2 were flat steel plate specimens. For specimen

SPP1, when loaded to approximately $0.95N_m$, local buckling occurred on the lower middle of outer steel plate. When the load reached the peak load of 550.3 kN (i.e. N_m), the lower middle of the inner steel plate buckled. The local buckling position of the specimen SPP1 occurred between two rows of studs, and the vertical displacements of each stud were consistent, and there was no damage to the concrete between the studs. The final failure mode of specimen SPP1 is illustrated in Fig. 7e. For specimen SPP2, when loaded to approximately $0.88N_m$, the upper left part of the outer steel plate buckled. When the load continued to increase, the upper left part of the inner steel plate buckled. When loaded to the peak load N_m, the upper right part of the inner and outer steel plates buckled. For specimen SPP2, because the concrete only provided out-of-plane support for the steel plates, there was no damage to the concrete. The final failure mode of SPP2 is illustrated in Fig. 7f.

3.2. Normalised average stress-strain curves

Fig. 8 shows the normalised average stress-strain curves of SCS sandwich composite tower specimens with different spacing-to-thickness ratios. The spacing-to-thickness ratios of specimens SPB2, SPB4 and SPB3 were 109, 65, and 32, respectively, and the corresponding spacing of the studs was 250, 200, and 150 mm, respectively. As reported in Fig. 8, the peak strength tends to increase with a decrease in the spacing-to-thickness ratio, especially for the specimen with the smaller spacing-to-thickness ratio. Fig. 9 shows the effect of the steel plate curvature radius on the peak strength of the specimens. As presented in Fig. 9, a steel plate with a small curvature radius has a larger peak strength. This is because when the curvature radius of the steel plate decreases, the out-of-plane stiffness of the steel plate increases, the stability of the steel plate is improved, and the peak strength increases accordingly.
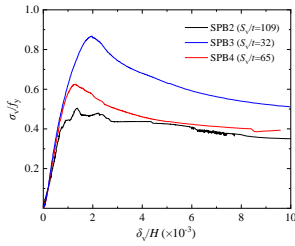

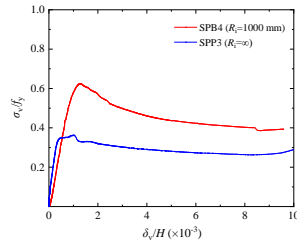**Fig. 8** Effect of S_v/t on the peak strength

Fig. 9 Effect of steel plate curvature radius on the peak strength

3.3. Load-strain curves

Using SPB2 as an example, the load-strain curve of the specimen was analysed. Fig. 10 presents the load-strain curve of the measuring point at the instability failure position of specimen SPB2, where "positive value" represents the tensile strain and "negative value" represents the compressive strain. As shown in Fig. 10, when the applied load is less than approximately 680 kN (equal to $0.88N_m$), the relationship between load and strain is basically linear. The experiments showed that there was an obvious local buckling that occurred in the steel plate when the load reached $0.88N_m$, resulting in the corresponding strain data of the inner and outer steel plates having an obvious mutation. According to the research results reported in literature [11], the load corresponding to the strain mutation point can be considered as the local buckling load of the steel plate. If the load-strain curve does not change, the load value corresponding to the first buckling of the steel plate is considered as the local buckling load of the steel plate. Similarly, local buckling loads of the inner and outer steel plates can be reached. The peak load (N_u), and the local buckling load of the inner steel plate (N_{li}), and outer steel plate (N_{lo}) of the specimens are listed in Table 3.
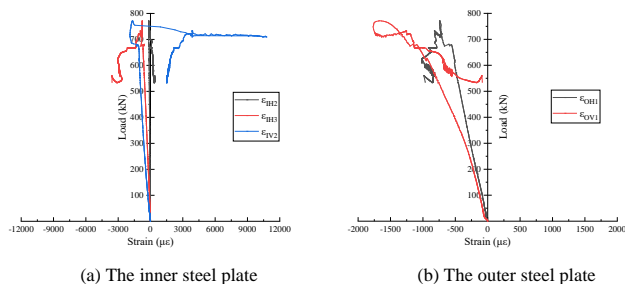

(a) The inner steel plate

(b) The outer steel plate

Fig. 10 Load-strain curves of specimen SPB2

Table 3

The peak load and local buckling load of specimens

Specimens	R_i (mm)	S_v/t (-)	N_u (kN)	N_{li} (kN)	N_{lo} (kN)
SPB1	1000	-	621.8	426.8	400.4
SPB2	1000	109	771.4	679.6	766.4
SPB3	1000	32	2432.8	2265.6	2398.3
SPB4	1000	65	955.2	800.6	857.0
SPP1	∞	66	550.3	503.8	528.5
SPP2	∞	-	544.9	527.7	481.8

4. Finite element analysis

4.1. Development of models

The ABAQUS package was employed for the FE element analysis. An ideal elastic-plastic constitutive model was adopted for the steel material. It can be seen from the experimental results that the load was applied only to the steel plate during the test, and the concrete only served as an out-of-plane support for the steel plate; therefore, an elastic constitutive model was adopted for the concrete. The elastic modulus of concrete was 32500 MPa, and the Poisson's ratio was 0.2. A gap was reserved between the concrete to consider the effect of 10mm thickness form boards with a negligible elastic modulus.

In the FE model, as shown in Fig. 11, S4R and C3D8R were selected to simulate the steel plate and concrete, respectively. To balance the calculation accuracy and efficiency of the FE model, a characteristic mesh element size of 20 mm for the steel plate and concrete was considered. In accordance with the test results, a linear elastic spring element was employed in the FE model to simplify the simulation of the studs. The stiffness of the studs along the length direction was 455.5 kN/mm, and the shear stiffness of the studs was not considered. The "surface-surface contact" was used to define the interface between steel plate and concrete, and the "hard contact" was used to simulate the normal behaviour interaction between the steel plate and concrete; the frictionless interaction was applied in the tangential direction. The top end of the specimen was completely fixed. The reference point RP-1 was introduced and coupled with the bottom surface of the steel plate to consider the effect of the endplate. Meanwhile, the lateral displacement of the reference point was limited (U1=U2=0), and the load was applied to the reference point RP-1.
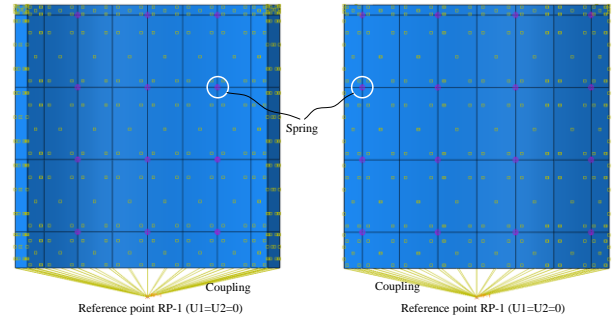

Fig. 11 Finite element modelling

In the FE model, the initial geometric imperfection and the initial eccentricity of the load of the specimens were introduced. Generally, there are two methods for considering the initial imperfections of the specimens. One is based on the eigenvalue buckling analysis results. In this method, the first buckling modes were selected as the initial imperfections of the specimens, and 1/1000 of the height of the specimen was set as the magnitude of the initial imperfections. The other method introduced the measured initial defect data of the specimen. In this study, the measured data of the initial out-of-plane deformation (see Fig. 12) of the steel plate were introduced into the model to consider the initial geometric imperfection.

The initial load eccentricity was applied by adjusting the position of the reference point RP-1, and the magnitude and direction of the eccentricity were determined by the following methods. Note that, in practical design and analysis, the initial imperfections caused by initial load eccentricity can not be considered.

Assuming that the axial load is N, and the eccentricity of the load toward the outer plate is ρ, as shown in Fig. 13, the centroid of the sections between the centre points A and B of the steel plate are y_1 and y_2, respectively. Then, the vertical stress of the steel plate at positions A and B in the elastic stage can be

expressed as:

$$\sigma_A = \frac{N}{A} + \frac{N\rho y_1}{I}$$
$$\sigma_B = \frac{N}{A} - \frac{N\rho y_2}{I} \tag{1}$$

where, A is the sectional area of the steel plate, and I is the moment of inertia of the section. According to Hooke's law, the vertical strain of the steel plate at A and B in the elastic stage can be obtained using Eq. (2), where E_s is the elastic modulus of the steel.

$$\varepsilon_A = \frac{\sigma_A}{E_s}$$
$$\varepsilon_B = \frac{\sigma_B}{E_s} \tag{2}$$

Then, the initial load eccentricity of the specimen can be obtained as follows:

$$\rho = \frac{2I}{A} \frac{1}{\frac{\varepsilon_A + \varepsilon_B}{\varepsilon_A - \varepsilon_B}(y_1 + y_2) - (y_1 - y_2)} \tag{3}$$

The initial eccentricity of the load was determined by calculating the strain data at the same height as the centreline of the inner and outer steel plates. The initial eccentricity, ρ, of the load was obtained by averaging the initial eccentricity at each height. The initial eccentricities of the load of the specimens are listed in Table 2.
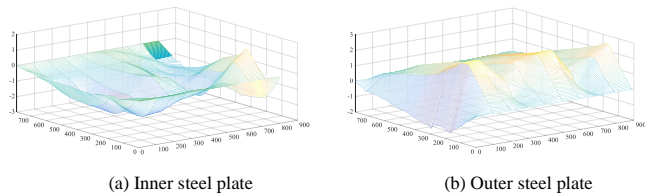

(a) Inner steel plate   (b) Outer steel plate

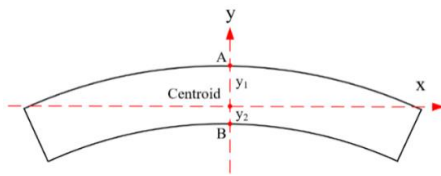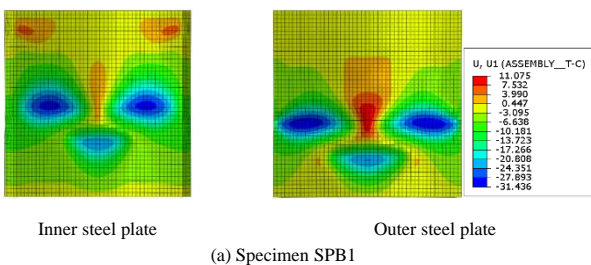**Fig. 12** Measured geometric imperfections of specimen SPB1

Fig. 13 Calculation and analysis diagram of load initial eccentricity

4.2. Model validation

4.2.1. Failure modes

Fig. 14 shows the failure modes of the specimens obtained from the FE modelling. Although the initial geometric imperfection and eccentricity of the load were introduced in the FE model, the FE model did not consider the influence of residual stress and the initially introduced geometric imperfection and eccentricity of the load were not identical to those of the specimens. Therefore, the above factors lead to slight differences between the numerical and experimental results. In general, the failure modes obtained from the FE results are in good agreement with the test results.

Inner steel plate   Outer steel plate

(a) Specimen SPB1

Inner steel plate   Outer steel plate

(b) Specimen SPB2

Inner steel plate   Outer steel plate

(c) Specimen SPB3

Inner steel plate   Outer steel plate

(d) Specimen SPB4

Inner steel plate   Outer steel plate

(e) Specimen SPP1

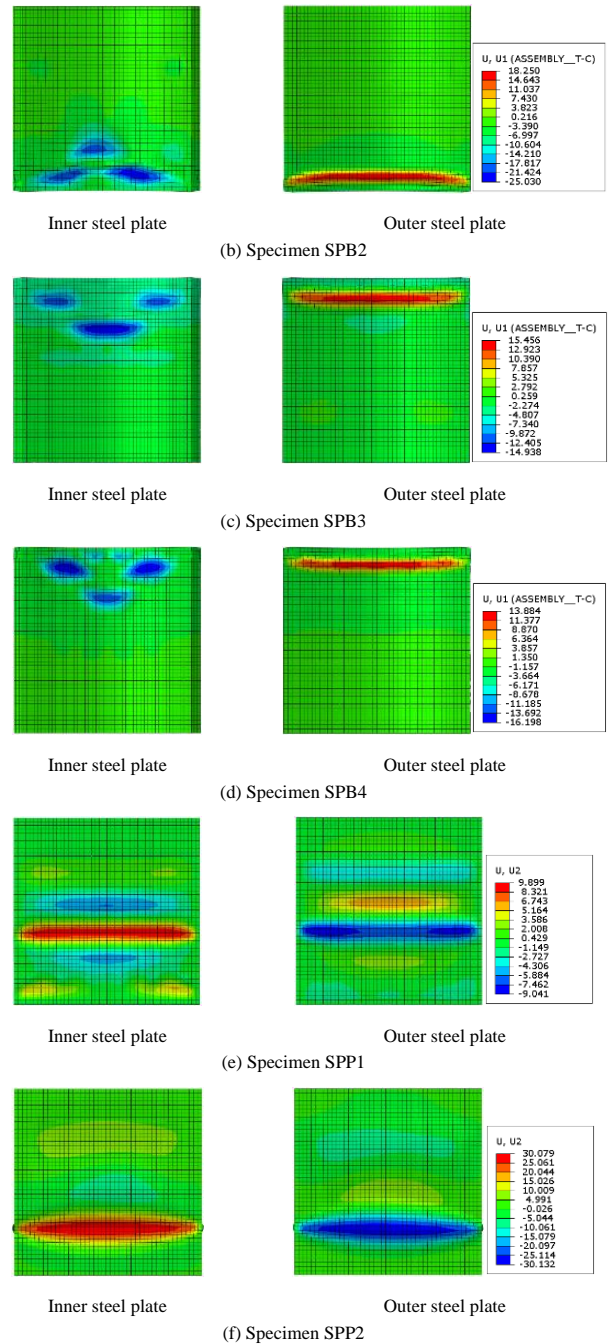Inner steel plate   Outer steel plate

(f) Specimen SPP2

Fig. 14 Failure modes of specimens obtained from FE modelling

4.2.2. Load-displacement curves

Fig. 15 shows a comparison of the load-displacement curves between the test and FE results and Table 4 shows the comparison of the bearing capacity between the test and FE results. Owing to the manufacturing defects and measurement deviations of the specimens, there might be a slight difference between the FE results and the test results. However, the FE model accurately simulate the bearing capacity and elastic stiffness of the specimens. Therefore, it can be observed that the FE model is in good agreement with the experimental results.
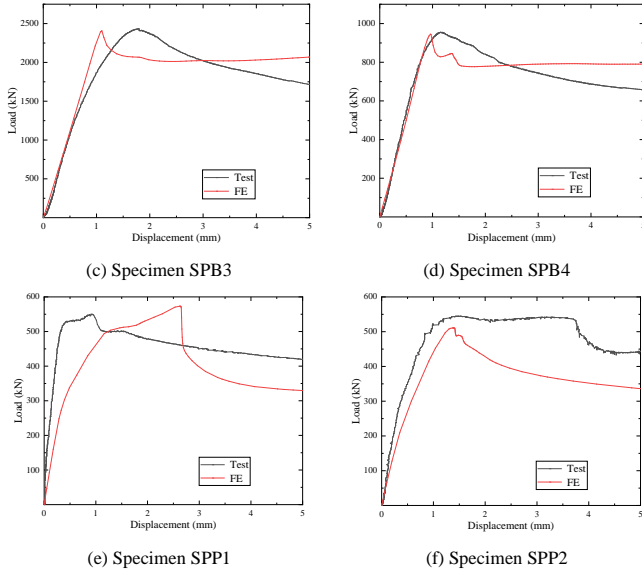

(a) Specimen SPB1   (b) Specimen SPB2

(c) Specimen SPB3
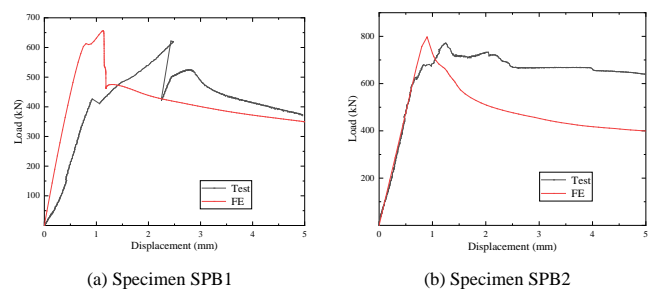
(d) Specimen SPB4

(e) Specimen SPP1

(f) Specimen SPP2

Fig. 15 Comparison of load-displacement curves between test and FE results

Table 4
Comparison of bearing capacity between test and FE results

	Specimens	SPB1	SPB2	SPB3	SPB4	SPP1	SPP2
Bearing capacity	Test (kN)	621.8	771.4	2432.8	955.2	550.2	544.9
	FE (kN)	655.9	797.7	2407.3	945.2	573.1	510.9
	FE/Test	1.05	1.03	0.99	0.99	1.04	0.94

5. Parametric study

According to the failure mode of the specimens of the SCS sandwich composite tower, the local buckling of the steel plate only occurred in all specimens between two rows of studs. Therefore, in this study, the stud was regarded as the supporting point of the steel plate, and the steel plate within the spacing of the studs was considered as the axial compression member, as shown in Fig. 16. The critical elastic buckling load (P_{cr}) of the steel plate was calculated using the following Eq. (4).

$$P_{cr} = \frac{\pi^2 E_s I}{(kl)^2} \tag{4}$$

where, E_s is the elastic modulus of the steel plate; I is the moment of inertia of the section; k is the effective length factor of the steel plate.

As shown in Fig. 16, the thickness of the steel plate is t, the vertical spacing of the studs is S_v, and the horizontal spacing is S_h. Then, the critical elastic buckling load of the steel plate can be obtained from Eq. (5):

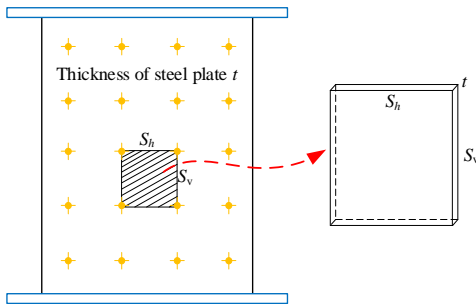$$P_{cr} = \frac{\pi^2 E_s (t^3 S_h / 12)}{(kS_v)^2} \tag{5}$$

Fig. 16 Elastic buckling stress model of steel plate

The corresponding critical stress of elastic buckling is:

$$\sigma_{cr} = \frac{P_{cr}}{A} = \frac{\pi^2 E_s (t^3 S_h / 12)}{(kS_v)^2 (tS_h)} = \frac{\pi^2 E_s}{12k^2 \left(\frac{S_v}{t}\right)^2} \tag{6}$$

According to Eq. (6), the effective length factor k is an important factor affecting the critical stress of the elastic buckling of the steel plate; therefore, it is necessary to study the effective length coefficient. In this study, the key parameters affecting the effective length factor of steel plates in SCS sandwich composite towers are the curvature radius of the steel plate, the thickness of the steel plate and the spacing of the studs. Therefore, in the parametric study, the effect of the above key parameters on the effective length factor of the SCS sandwich composite tower is analysed, which is expected to provide a basis for the proposal of a design method for the effective length factor.

5.1. Finite element model of tower structure

To accurately simulate the critical elastic buckling stress of a steel plate in an actual tower structure, an FE model was established to analyse the critical elastic buckling stress of the steel plate in the SCS sandwich composite tower. Owing to the support provided by the core concrete to the inner and outer steel plates, the buckling and deformation directions of the inner and outer steel plates are different, which leads to different local stabilities of the inner and outer steel plates. Therefore, in a parametric study, the inner and outer steel plates should be studied separately.

In the parametric study, the parameters of the FE model of the tower structure (see Fig. 17) are the same as those of the above-mentioned specimen FE model, but it should be noted that: (1) the eigenvalue buckling analysis is used to obtain the critical elastic buckling load of the steel plate, and the effective length factor of the steel plate can be obtained by calculating the critical elastic buckling stress using Eq. (6); (2) the vertical and horizontal spacing of the studs in all the FE models is equal; (3) The heights of all specimens were set as 6-10 times the spacing of the studs to eliminate the influence of boundary conditions on the FE analysis results.
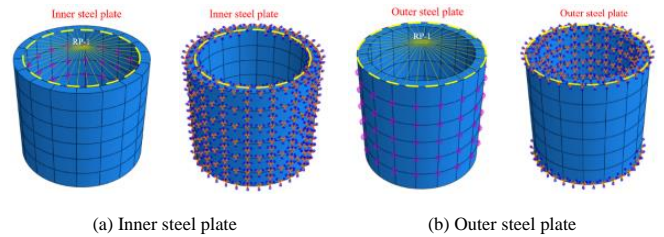

(a) Inner steel plate

(b) Outer steel plate

Fig. 17 FE model of SCS sandwich composite tower

5.2. Effect of the stud spacing

In the parametric study, the spacing of the studs of the inner and outer steel plates was considered as S_v = 100, 115, 133 and 150 mm. Fig. 18 shows the effect of the stud spacing on the effective length factor of the inner and outer steel plates. It can be seen that the effective length factor of the inner and outer steel plates decreasing trend is basically the same. With an increase in the stud spacing, the effective length factor decreases, and the outer steel plate has a larger effective length factor than that of the inner steel plate.
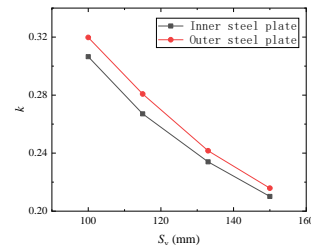

Fig. 18 Effect of the stud spacing on the effective length factor

5.3. Effect of the steel plate thickness

In the parametric study, steel plate thicknesses (t) of 2, 3, 4, and 5 mm were considered. The effect of the steel plate thickness on the effective length factor is shown in Fig. 19. As shown in Fig. 19, for a steel plate of the same thickness, the effective length factor of the outer steel plate is greater than that of the inner steel plate. The increase in the thickness of the steel plate has a positive effect on the effective length factor, especially for the outer steel plate. The effect of the spacing-to-thickness ratio S_v/t on the effective length factor is shown in Fig. 20. As illustrated in Fig. 20, with an increase in the spacing-to-thickness ratio,

the effective length factor decreases and the influence of the spacing-to-thickness ratio on the effective length factor of the inner and outer steel plates is similar. The effective length factor of the outer steel plate was greater than that of the inner steel plate with the same spacing-to-thickness ratio.
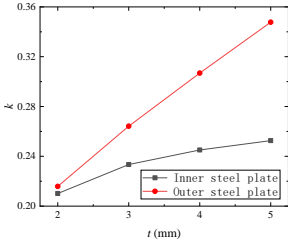

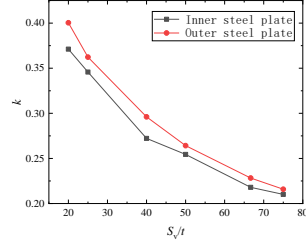**Fig. 19** Effect of steel plate thickness on the effective length factor

Fig. 20 Effect of S_v/t on the effective length factor

5.4. Effect of the steel plate curvature radius

In the parametric study, the steel plate curvature radius ranged between 400 and 1000 mm at 200 mm intervals. Fig. 21 shows the effect of the steel plate curvature radius on the effective length factor. With an increase in the curvature radius of the steel plate, the effective length factors increase. The effective length factors of the outer steel plate are generally larger than those of the inner steel plate, and the increase in the effective length factors of the outer steel plate is greater. This is because when the curvature radius of the steel plate increases, the local stability of steel plate becomes worse, and the steel plate is more prone to local instability failure. The effect of S_v/R on the effective length factor is shown in Fig. 22. As shown in Fig. 22, the effective length factor of the steel plate is smaller when the S_v/R becomes larger, and the effective length factor of the outer steel plate is larger than that of the inner steel plate and the trends of the two curves are similar.
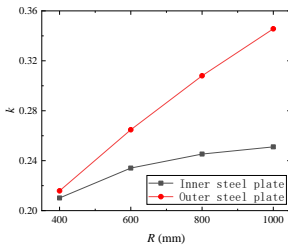

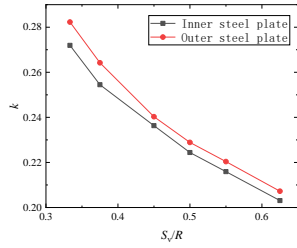**Fig. 21** Effect of steel plate curvature radius on the effective length factor

Fig. 22 Effect of S_v/R on the effective length factor

6. Development of design rules

In this study, the critical stress of elastic buckling of a steel plate was analysed based on the column stability theory. The integral FE model of the actual tower structure was developed based on the validated FE model and actual tower structure form. The influence of the curvature radius of the steel plate, thickness of the steel plate and vertical spacing of the stud on the effective length factor of the inner and outer steel plates were studied. From the results of the parametric analysis, it can be seen that the governing parameters of the effective length factors of the inner and outer steel plates are the spacing-to-thickness ratio S_v/t and the spacing-to-curvature radius of the steel plate S_v/R, and the effective length factors of the inner and outer steel plates are smaller when the spacing-to-thickness ratios S_v/t and S_v/R have larger values. Note that S_v/t and S_v/R are dimensionless coefficients, which can effectively eliminate the influence of the size effect on the analysis results. When the curvature radius of the steel plate tends to infinity (i.e. the flat steel plate), the effective length factor of the flat steel plate proposed by Yan et al. [10] is 0.825. Because the steel plate of the SCS sandwich composite tower is curved, l the local stability of the steel plate with curvature is different from that of the flat steel plate, and the effective length factor k is no longer a constant value for the steel plate with curvature.

In the form of Eq. (6), based on the newly generated 240 FE analysis results, the design method of the effective length factor k for the inner and outer steel plates of the SCS sandwich composite tower is achieved through linear regression, as follows:

Inner steel plate:

$$k = \frac{1}{0.5170\left(\frac{S_v}{R}\right)^{0.45}\left(\frac{S_v}{t}\right)^{0.55}+1.212} \tag{7}$$

Outer steel plate：

$$k = \frac{1}{0.2316\left(\frac{S_v}{R}\right)^{1.1}\left(\frac{S_v}{t}\right)^{0.9}+1.212} \tag{8}$$

Fig. 23 shows a comparison of the effective length factor calculated using Eq. (7) and the FE analysis results, and good agreement was observed between the predicted and the numerical results. As shown in Fig. 23, the mean values of predicted results to the numerical results of the inner and outer steel plates were 1.01 and 1.00 respectively, and the coefficients of variation (COV) of the inner and outer steel plates were 0.0026 and 0.0082 respectively. This indicates that the proposed design method can provide accurate and consistent predictions.

Substituting Eqs. (7) and (8) into Eq. (6), the design method for calculating the critical elastic buckling stress of the inner and outer steel plates can be obtained as follows:

Inner steel plate:

$$\sigma_{cri} = \frac{\pi^2 E_s \left(0.5170\left(\frac{S_v}{R}\right)^{0.45}\left(\frac{S_v}{t}\right)^{0.55}+1.212\right)^2}{12\left(\frac{S_v}{t}\right)^2} \tag{9}$$

Outer steel plate：

$$\sigma_{cro} = \frac{\pi^2 E_s \left(0.2316\left(\frac{S_v}{R}\right)^{1.1}\left(\frac{S_v}{t}\right)^{0.9}+1.212\right)^2}{12\left(\frac{S_v}{t}\right)^2} \tag{10}$$

If the critical elastic buckling stress is no less than the yield strength of the steel plate, that is, no buckling occurs before the steel plate yields, then the limit design method of the spacing of the studs of the inner steel plate can be obtained as follows:

Inner steel plate:

$$S_{vi} \leq \frac{1.212}{\sqrt{\frac{12 f_y}{\pi^2 E_s t^2}}-\frac{0.5170}{R^{0.45}t^{0.55}}} \tag{11}$$

Outer steel plate：

$$S_{vo} \leq \frac{1.212}{\sqrt{\frac{12 f_y}{\pi^2 E_s t^2}}-\frac{0.2316}{R^{1.1}t^{0.9}}} \tag{12}$$

(a) Inner steel plate
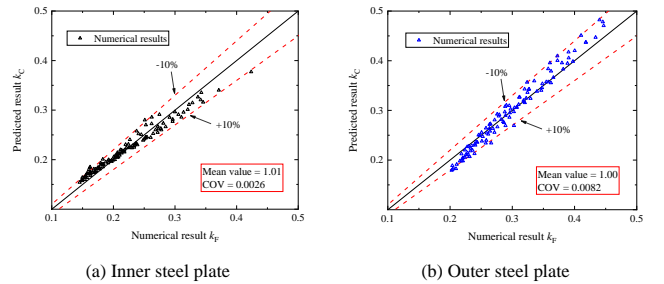
(b) Outer steel plate

Fig. 23 Comparison between formula calculation value k_C and FE value k_F

7. Conclusions

Six specimens of SCS sandwich composite towers were tested under axial compression, and FE models were employed and validated against the test results. The test results showed the following: (1) in all the specimens the local failure mode occurred between the studs; (2) the peak strength of the steel plate increased with a decrease in the curvature radius of the steel plate and a decrease in the spacing-to-thickness ratio; (3) the peak strength of the steel plate increased with a decrease in the spacing-to-thickness ratio (the decrease of the spacing of the studs and the increase of the thickness of the steel plate), and the influence of the thickness of the steel plate on the peak strength was more significant. An FE model of the tower structure was developed to analyse the critical elastic buckling stress of the steel plate in the SCS sandwich composite

tower. The influence of three parameters (curvature radius of the steel plate, thickness of the steel plate, and the spacing of the studs) on the effective length factors of the inner and outer steel plates was studied. Based on the parameter analysis results, the design rules of the effective length factor of the inner and outer steel plates, and design methods for the spacing of studs to prevent local instability of the inner and outer steel plates before yielding were proposed. The outcome of this study provides a theoretical basis and design guidance for the application of SCS sandwich composite structures in the field of wind power generation.

Acknowledgments

References

[1] Pan F.S., Wang F.W., Ke S.T. and Tang G., Buckling analysis and stability design of wind turbine tower with geometic imperfections, Acta Energiae Solaris Sinica, 10, 2659-2664, 2017.

[2] Wang S.Y., Chen A.Y. and Wan H.Y., Seismic behaviour of concrete-filled steel tube frames with external composite wall panels, Advanced Steel Construction, 17(1), 10-19, 2021.

[3] Wang Z., Yan J.B. and Liu X.M., Numerical and theoretical studies on double steel plate composite walls under compression at low temperatures, Advanced Steel Construction, 17(4), 376-384, 2021.

[4] Qi Y., Gu Q., Sun G.H., Zhao B.C. and Wang H.F., Tensile force and bending moment demands on headed stud for the design of composite steel plate shear wall, Advanced Steel Construction, 15(4), 338-348, 2019.

[5] Yan J.B., Wang Z. and Wang X., Behaviour of steel-concrete-steel sandwich plates under different ice-contact pressure, Advanced Steel Construction, 15(1), 116-122, 2019.

[6] Liu S.M., Ding H.S., Taerwe L. and De Corte W., Modifications to the global and interactive shear buckling analysis methods of trapezoidal corrugated steel webs for bridges, Advanced Steel Construction, 15(4), 349-363, 2019.

[7] Choi B.J., Kim W.K., Kim W.B. and Kang C.K., Compressive performance with variation of yield strength and width-thickness ratio for steel plate-concrete wall structures, Steel and Composite Structures, 14(5), 473-491, 2013.

[8] Choi B.J., Kang C.K., and Park H.Y., Strength and behavior of steel plate–concrete wall structures using ordinary and eco-oriented cement concrete under axial compression, Thin-Walled Structures, 84, 313-324, 2014.

[9] Kang C.K., Choi B.J., and Jeoung B.S., Compressive Behavior of Steel Plate-Concrete Structures using Eco-Oriented Cement Concrete. Journal of Korean Society of Steel Construction, 24(5), 583, 2012.

[10] Yan J.B., Wang Z., Luo Y.B. and Wang T., Compressive behaviours of novel SCS sandwich composite walls with normal weight concrete. Thin-Walled Structures, 141, 119-132, 2019.

[11] Yang Y., Liu J. and Fan J., Buckling behavior of double-skin composite walls: an experimental and modeling study, Journal of Constructional Steel Research, 121, 126-135, 2016.

[12] Uy B. and Bradford M.A., Local buckling of thin steel plates in composite construction: experimental and theoretical study, Structure and Buildings,110(4), 426-440,1995.

[13] Uy B. and Bradford M.A., Elastic local buckling of steel plates in composite steel-concrete members, Engineering Structures, 18(3), 193-200, 1996.

[14] Cai J. and Long Y.L., Local Buckling Of Steel Plates In Rectangular CFT Columns With Binding Bars. Journal of Constructional Steel Research, 65(4), 965-972, 2009.

[15] Hu H.S., Fang P.P., Liu Y., Guo Z.X. and Shahrooz B.M., Local buckling of steel plates in composite members with tie bars under axial compression, Engineering Structures, 205, 110097, 2020.